https://doi.org/10.37434/tpwj2020.10.05

INFLUENCE OF AMPLITUDE AND FREQUENCY OF OSCILLATIONS OF ELECTRODE WIRE IN ARC SURFACING ON FORMATION AND STRUCTURE OF THE DEPOSITED METAL AND PENETRATION OF BASE METAL

A.A. Babinets, I.O. Ryabtsev, I.P. Lentyugov, I.I. Ryabtsev, T.V. Kaida and **I.I. Bogaichuk**
E.O. Paton Electric Welding Institute of the NAS of Ukraine
11 Kazymyr Malevych Str., 03150, Kyiv, Ukraine. E-mail: office@paton.kiev.ua

The influence of amplitude and frequency of oscillations of electrode wire during arc surfacing on formation of deposited beads, nature of base metal penetration, as well as structural and chemical heterogeneity in the zone of the joint of deposited and base metals were studied. It was established that an increase in the frequency of oscillations of electrode wire, at the same amplitude of oscillations and rate of deposition, leads to an improvement in formation of the deposited metal and mixing of the layers in the deposited metal; formation of a more dispersed structure; narrowing of the transition zone; more uniform distribution of alloying elements; more uniform penetration and «smoothing» of the fusion boundary of the deposited and base metal. The mentioned regularities almost do not change with an increase in the amplitude of oscillations. It was established that the best formation of the deposited metal occurs at the maximum frequency N = 45 min^{-1} and amplitude of oscillations of the electrode wire A = 25 mm and deposition rate V_d = 7 m/h. 8 Ref., 2 Tables, 10 Figures.

Keywords: arc surfacing, electrode wire oscillation, amplitude and frequency of oscillations, base metal penetration, deposited metal formation, deposited metal structure, structure heterogeneity

Large penetration of base metal is one of the disadvantages of arc surfacing. In order to reduce base metal penetration and obtain wide and relatively low beads, it is proposed to perform arc surfacing with oscillations of electrode wire or strip [1–6]. In these works, the conclusions on the positive impact of oscillations of electrode wire or strip on the extent and nature of base metal penetration were evaluated, mainly, on transverse sections of the deposited beads, and the impact of electrode wire oscillation on structural heterogeneity of the deposited metal was not studied, either.

However, considering the fact of direct impact of the arc on base metal during transverse oscillations of electrode wire and its displacement in the longitudinal direction, it is to be anticipated that the nature of penetration in the longitudinal and transverse sections of the deposited beads can change. This fact should be taken into account at development of the technologies of deposition of parts, operating not only under the conditions of different kinds of wear, but also cyclic loading, as nonuniform penetration can lead to lowering of their wear resistance, as well as fatigue life at cyclic mechanical and thermal loads [7, 8].

Analysis shows that in this case, if we ignore the electric parameters of the surfacing mode, the main effect on base metal penetration, formation and structure of the deposited beads is produced by amplitude and frequency of oscillations of electrode wire or strip, as well as the deposition rate. These three characteristics are interconnected, and at the change of one of them, the others should be adjusted, in order to obtain sound deposited beads.

Thus, the objective of the experiments was studying the impact of the frequency and amplitude of oscillations of electrode wire at arc surfacing, as well as the deposition rate on base metal formation, depth and nature of base metal penetration, its fraction in the deposited metal and on the deposited metal structure. Investigations were conducted on longitudinal and transverse sections of the deposited beads.

Flux-cored wire of PP-Np-30Kh20MN type of 2.6 mm diameter was used as the model material. Surfacing was performed using AN-26P flux. Surfacing modes were as follows: current of 280–320 A; voltage of 30–32 V; deposition rate of 7 and 10 m/h; oscillation frequency, N of 18; 28; 32 and 45 min^{-1}; os-

A.A. Babinets — https://orsid.org/0000-0003-4432-8879, I.O. Ryabtsev — https://orsid.org/0000-0001-7180-7782,
I.P. Lentyugov — https://orsid.org/0000-0001-8474-6819, I.I. Ryabtsev — https://orsid.org/0000-0001-7550-1887

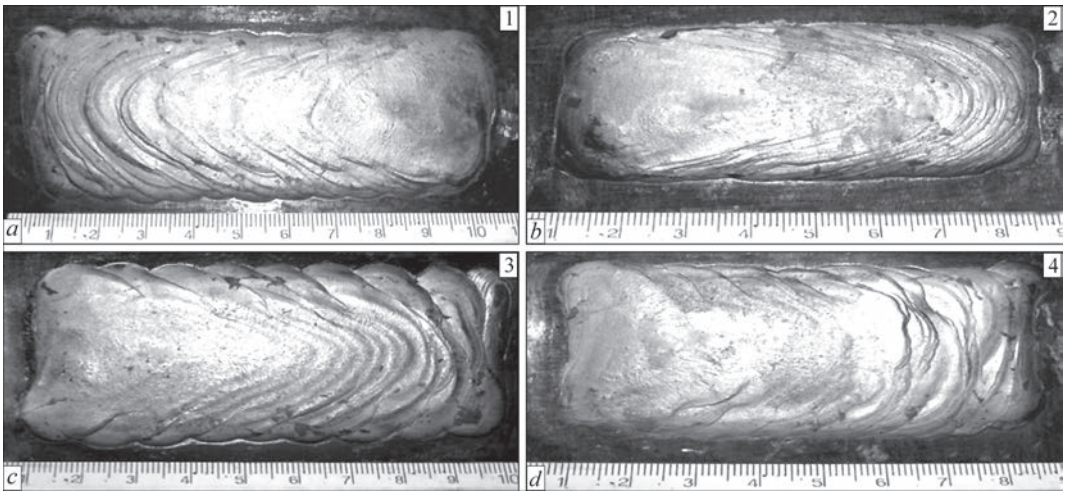

Figure 1. Appearance of beads, deposited at rate V_d = 7 m/h; *a* — sample 1: *A* = 25 mm; *N* = 28 min^{-1}; *b* — sample 2: *A* = 25 mm; *N* = 45 min^{-1}; *c* — sample 3: *A* = 40 mm; *N* = 18 min^{-1}; *d* — sample 4: *A* = 40 mm; *N* = 32 min^{-1} (for sample numbers see Table 1)

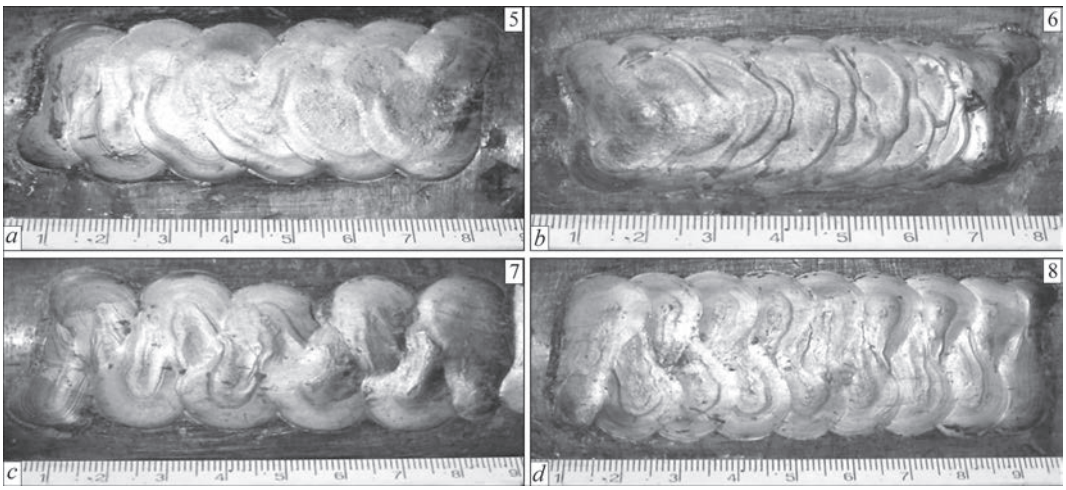

Figure 2. Appearance of beads, deposited at rate V_d = 10 m/h; *a* — sample 5; *A* = 25 mm; *N* = 28 min^{-1}; *b* — sample 6: *A* = 25 mm; *N* = 45 min^{-1}; *c* — sample 7: *A* = 40 mm; *N* = 18 min^{-1}; *d* — sample 8: *A* = 40 mm; *N* = 32 min^{-1} (for sample numbers see Table 1)

cillation amplitude, *A* — 25 and 40 mm. Altogether, 8 samples were deposited for investigations.

The beginning and crater part were cut off the deposited beads (Figures 1, 2). Longitudinal and transverse macrosections were cut out of the remaining material, in order to determine the size of the beads, base metal penetration and its proportion in the deposited metal γ_O (PBM) (Table 1), as well as for studying the macro- and microstructure of the deposited beads.

$$\gamma_0 = \frac{F_b}{F_b + F_d} \cdot 100\ \%,$$

where F_b and F_d are the cross-sectional areas of the base and deposited metals, respectively.

Table 1. Influence of deposition mode on geometrical parameters of the beads

Sample number	Oscillation		Deposition rate, m/h	Bead dimensions, mm			PBM, %
	Amplitude *A*, mm	Frequency *N*, min^{-1}		Width	Height	Penetration depth	
1	25	28	7	38.8	3.4	1.7	39
2*	25	45	7	36.4	2.95	1.6	37
3	40	18	7	46.8	2.05	1.8	54
4	40	32	7	47.0	1.8	1.5	50
5	25	28	10	37.5	1.9	1.8	55
6	25	45	10	35.8	2.7	1.5	52
7	40	18	10	42.6	2.1	1.5	50
8	40	32	10	44.7	1.5	1.4	49

*Sample, deposited in the mode providing the optimum result.

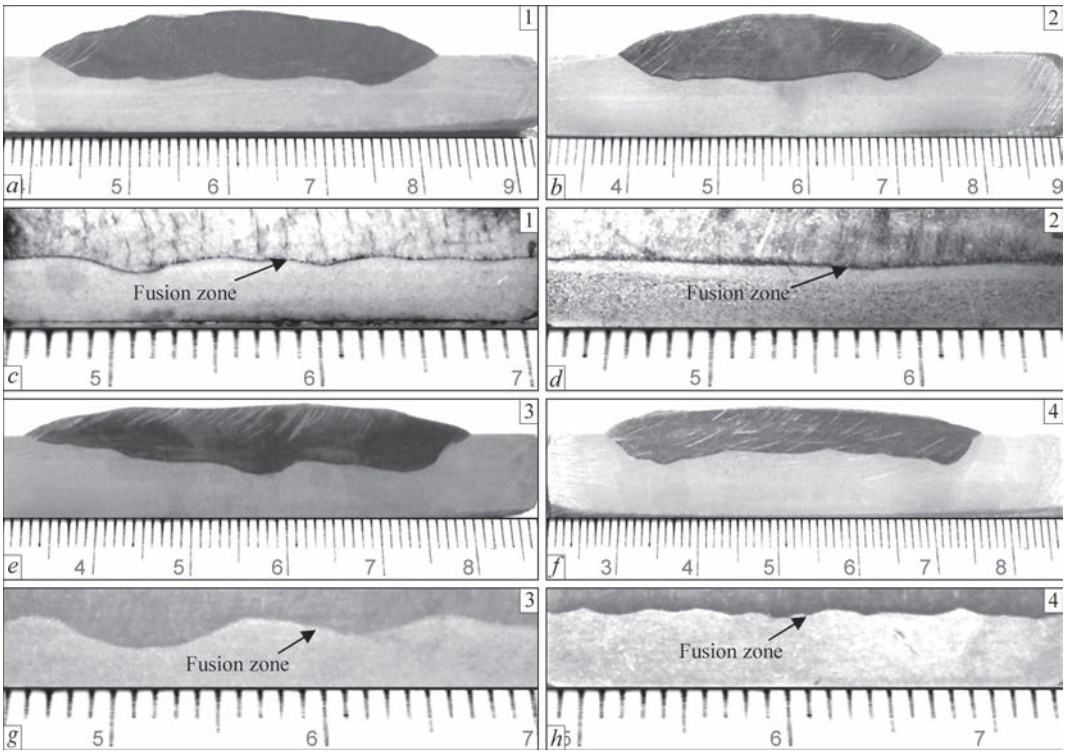

Figure 3. Transverse (*a*, *b*, *e*, *f*) and longitudinal (*c*, *d*, *g*, *h*) macrosections of samples, deposited at the rate of 7 m/h: *a*, *c* — sample 1: A = 25 mm; N = 28 min^{-1}; *b*, *d* — sample 2: A = 25 mm; N = 45 min^{-1}; *e*, *g* — sample 3: A = 40 mm; N = 18 min^{-1}; *f*, *h* — sample 4: A = 40 mm; N = 32 min^{-1} (for sample numbers see Table 1)

Minimum PBM on the level of 37–39 % was found in samples Nos 1 and 2, penetration depth was 1.6–1.7 mm. Smaller penetration value of 1.4–1.5 mm was noted in samples Nos 7 and 8. However, PBM in these samples is on the level of 49–50 % (Table 1).

Based on aggregate assessment of the deposited bead dimensions, penetration depth and PBM, the following mode was determined to be optimum: deposition rate of 7 m/h; amplitude of electrode wire oscillations A = 25 mm, its oscillation frequency N = = 45 min^{-1} (Table 1, sample 2).

Figure 3, *a*, *b*, *e*, *f* shows the photo of macrosections, cut out across, and Figure 3, *c*, *d*, *g*, *h* — those cut out along the longitudinal axis of the beads, deposited at the rate of 7 m/h. Accordingly, Figure 4, *a*, *b*, *e*, *f* shows the photo of macrosections, cut out across, and Figure 4, *c*, *d*, *g*, *h* — along the longitudinal axis of the beads, deposited at the rate of 10 m/h.

If we analyze the longitudinal macrosections, then at deposition rate of 7 m/h increase of the frequency of electrode wire oscillations promotes producing a more uniform penetration and smoother fusion boundary of the deposited and base metals (Figure 3, *d*, *h*). Here, the most even fusion boundary is achieved at oscillation amplitude of 25 mm and maximum frequency of 45 min^{-1} (Figure 3, *d*; Table 1, sample 2).

Transverse macrosections of the beads, deposited at the rate of 7 m/h with different oscillation parameters, differ only slightly one from another. It is worth noting just the macrosection in Figure 3, *f* (sample 4), which is characterized by minimum penetration of 1.5 mm.

At increase of deposition rate up to 10 m/h, a uniform penetration along the deposited beads could not be achieved at any of the frequencies and amplitudes of electrode wire (Figure 4, *c*, *d*, *g*, *h*). Here, at deposition at a higher rate (10 m/h), increase of oscillation frequency of electrode wire also promotes achieving a more uniform penetration and greater «smoothness» of the fusion line (Figure 4, *d*, *h*). This influence, however, is weaker than at the deposition rate of 7 m/h.

Similar to the rate of 7 m/h, nonuniform penetration is observed also in microsections, cut out across the beads, deposited at the rate of 10 m/h (Figure 4, *b*, *e*, *f*, samples 6, 7, 8).

Deposited metal of sample 1 (V_d = 7 m/h; A = = 25 mm; N = 28 min^{-1}) has a dendritic microstructure (Figure 5, *a*). Cellular solidification prevails in the subsurface layers of the deposited metal, with average cell size of 60–80 μm. Hardness of the matrix base is equal to $HV1$ = 5420–6060 MPa (martensite, residual austenite, carbides). Precipitation of chains of globular-shaped particles occurs along the crystallite boundaries (Figure 5, *b*).

Solidification of deposited metal of sample 2 (V_d = = 7 m/h; A = 25 mm; n = 45 min^{-1}) is dendritic-cellular with prevalence of the cellular type (Figure 5, *c*), with average cell size of 30–40 μm. Solidification

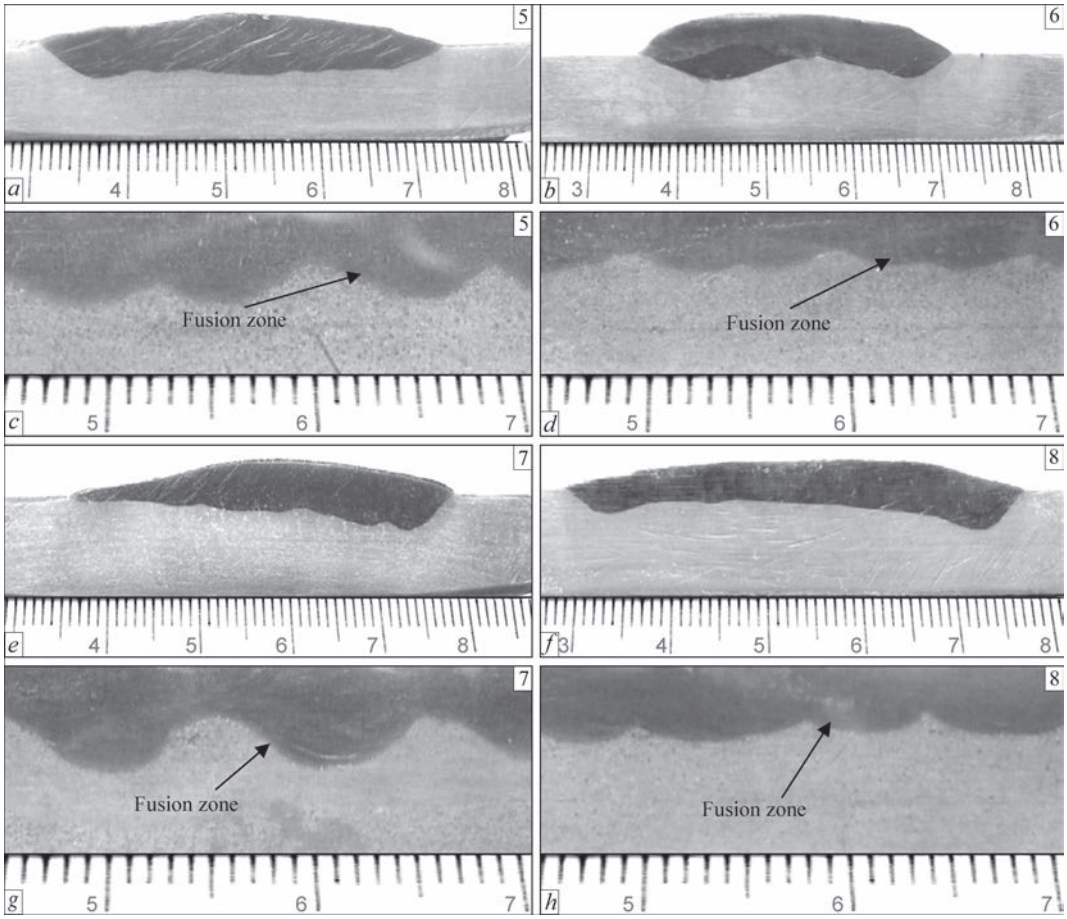

Figure 4. Transverse (*a*, *b*, *e*, *f*) and longitudinal (*c*, *d*, *g*, *h*) macrosections of samples, deposited at the rate of 10 m/h: *a*, *c* — sample 5: A = 25 mm; N = 28 min^{-1}; *b*, *d* — sample 6: A = 25 mm; N = 45 min^{-1}; *e*, *g* — sample 7: A = 40 mm; N = 18 min^{-1}; *f*, *h* — sample 8: A = 40 mm; N = 32 min^{-1} (for sample numbers see Table 1)

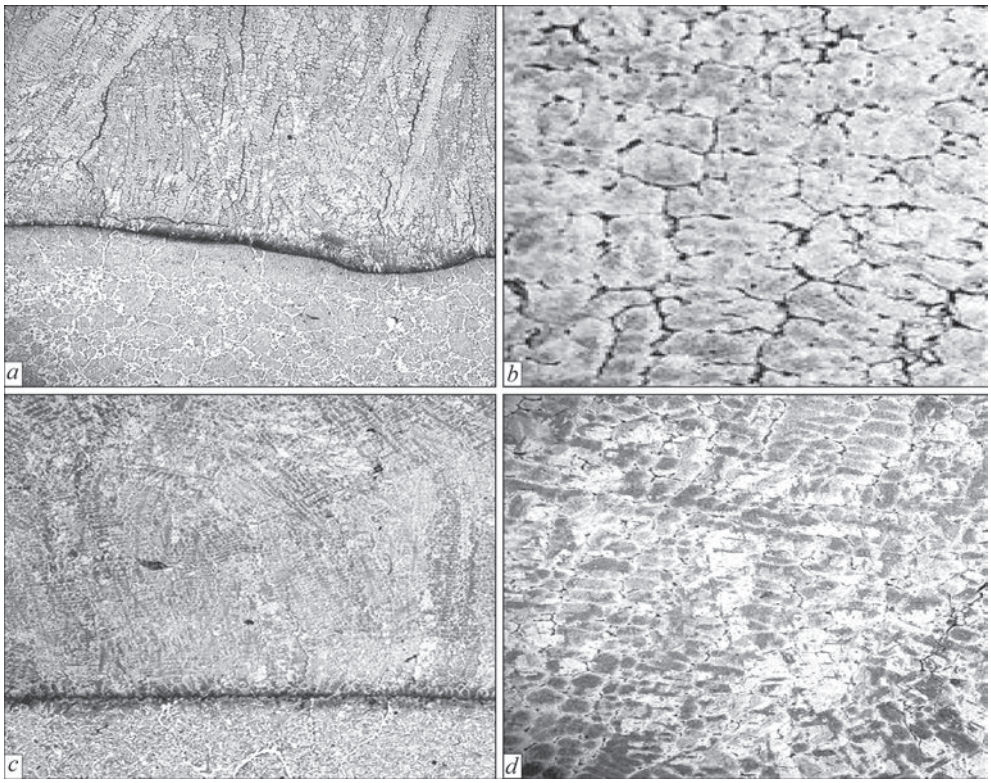

Figure 5. Microstructure of deposited metal of samples 1 (*a*, *b*) and 2 (*c*, *d*): *a*, *c* — fusion zone, ×20; *b*, *d* — deposited metal, ×100. Electrolytic etching in chromic acid. $U_{o.-c}$ = 20 V; t = 3–5 s (for sample numbers see Table 1)

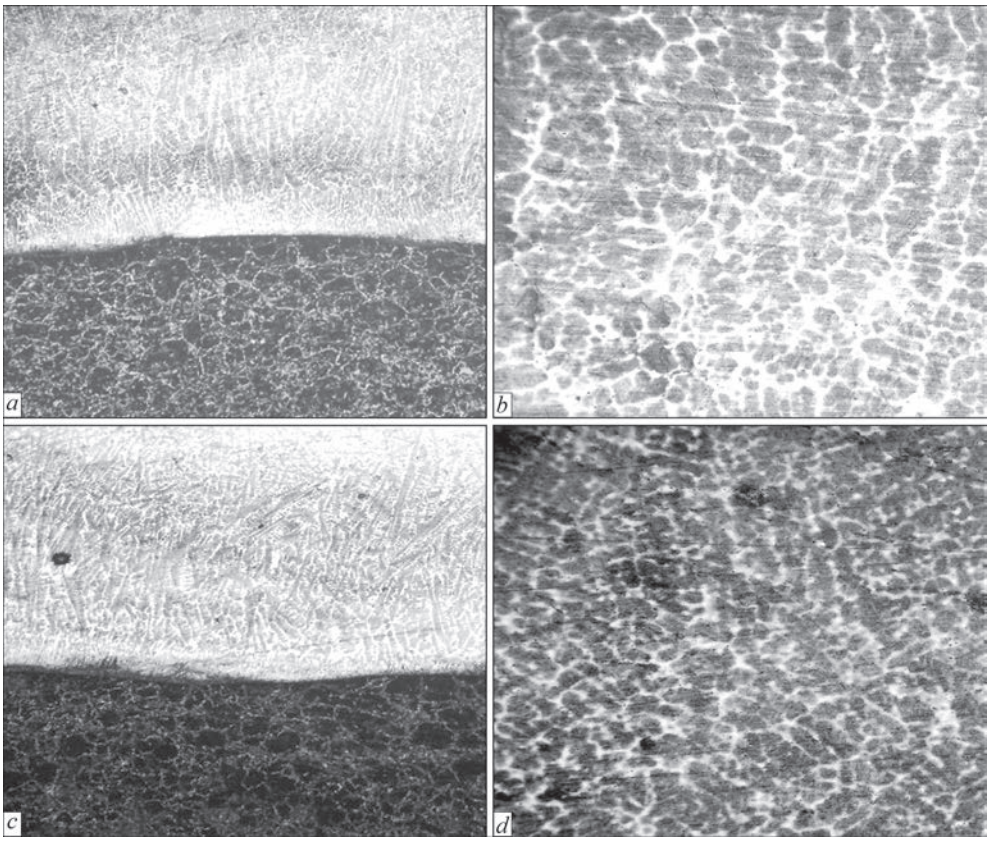

Figure 6. Microstructure of deposited metal of samples 3 (*a*, *b*) and 4 (*c*, *d*): *a*, *c* — fusion zone, ×20; *b*, *d* — deposited metal, ×100. Electrolytic etching in chromic acid. $U_{o\text{-}c}$ = 20 V; *t* = 3–5 s (for sample numbers see Table 1)

becomes dendritic at the line of fusion with the base metal. The width of crystallites in this region is equal to 70–90 μm. Hardness of the matrix base is *HV*1–4880–5480 MPa. Within the crystallites, similar to sample No.1, excess phase precipitates in the form of globular dispersed particles (Figure 5, *d*). HAZ width is equal to 3600 μm.

Microstructure of deposited metal of sample 3 (V_d = = 7 m/h; *A* = 40 mm; *N* = 18 min^{-1}) is dendritic-cellular with prevalence of the cellular one (Figure 6, *a*, *b*). Average diameter of the cells is 50–60 μm. Hardness of the matrix base is *HV*1–6060–6130 MPa. A martensite ridge is observed at the fusion line from the deposited metal side. In this zone, martensite forms large needles. Crystallite width at the fusion line is 70–80 μm. HAZ width is 2100 μm.

Deposited metal of sample 4 (V_d = 7 m/h; *A* = = 40 mm; *N* = 32 min^{-1}) also has dendritic-cellular structure with the cellular shape prevailing on the surface. Cell diameter is equal to 40–50 μm (Figure 6, *b*, *c*). The structure at the fusion line is dendritic, crystallite width in this region is 60–80 μm. Hardness inside the crystalline base in this sample is lower than that in sample 3 and is equal to *HV*1–5140–5420 MPa. HAZ width is 1800 μm.

Microstructural studies of sample 5 (V_d = 10 m/h; *A* = 25 mm; *N* = 28 min^{-1}) showed that it has a dendritic structure (Figure 7, *a*, *b*). Cellular solidification prevails in the subsurface layers of the deposited metal, with average cell diameter of 60–80 μm. Matrix base hardness is *HV*1–6860 MPa. Particles of a globular shape precipitate on the crystallite boundaries. Cell diameter in the upper part of the deposited metal is 15–20 μm; crystallite width h_{cryst} is 15–25 μm, HAZ width is 1200 μm. Intermetallic or carbide precipitates are observed along the crystallites boundaries.

Microstructure of sample 6 (V_d = 10 m/h; *A* = = 25 mm; *N* = 45 min^{-1}) is shown in 7, *c*, *d*. It also has a dendritic structure, with cellular solidification in the subsurface layers. Cell diameter is 25–35 μm; crystallite width h_{cryst} is 25–50 μm, HAZ width is 800–900 μm. Intermetallic or carbide precipitates are present along the boundaries of crystallites and cells. Microhardness is *HV*1–6810 MPa in the light layer and *HV*1–6340 MPa in the dark layer.

Microstructural studies of sample 7 (V_d = 10 m/h; *A* = 40 mm; *N* = 18 min^{-1}) showed that it has a dendritic-cellular structure (Figure 8, *a*, *b*). Cell diameter is 40–60 μm; crystallite width h_{cryst} is 40–60 μm, HAZ width is 1000–1200 μm. Microhardness is *HV*1–6420 MPa. There are some precipitates along the crystallite and cell boundaries, but their number is much smaller than in samples 5 and 6, shown in Figure 7.

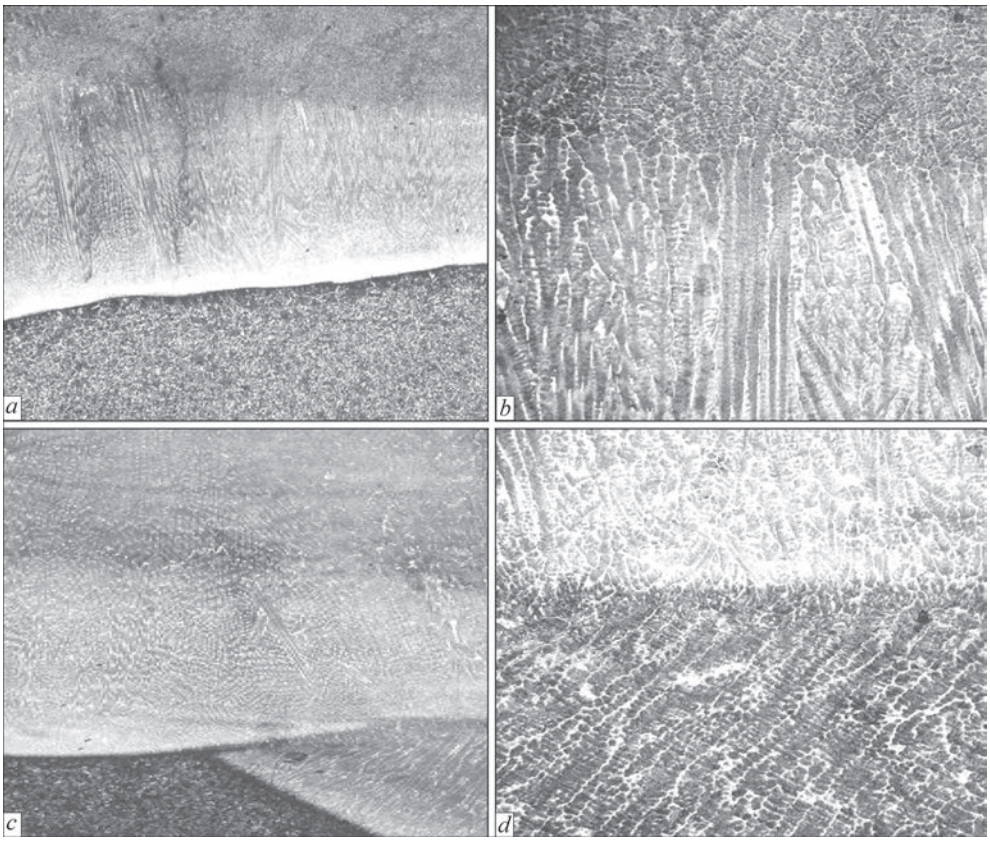

Figure 7. Microstructure of deposited metal of samples 5 (*a*, *b*) and 6 (*c*, *d*): *a*, *c* — fusion zone, ×20; *b*, *d* — deposited metal, ×100. Electrolytic etching in chromic acid. $U_{o.-c}$ = 20 V; *t* = 3–5 s (for sample numbers see Table 1)

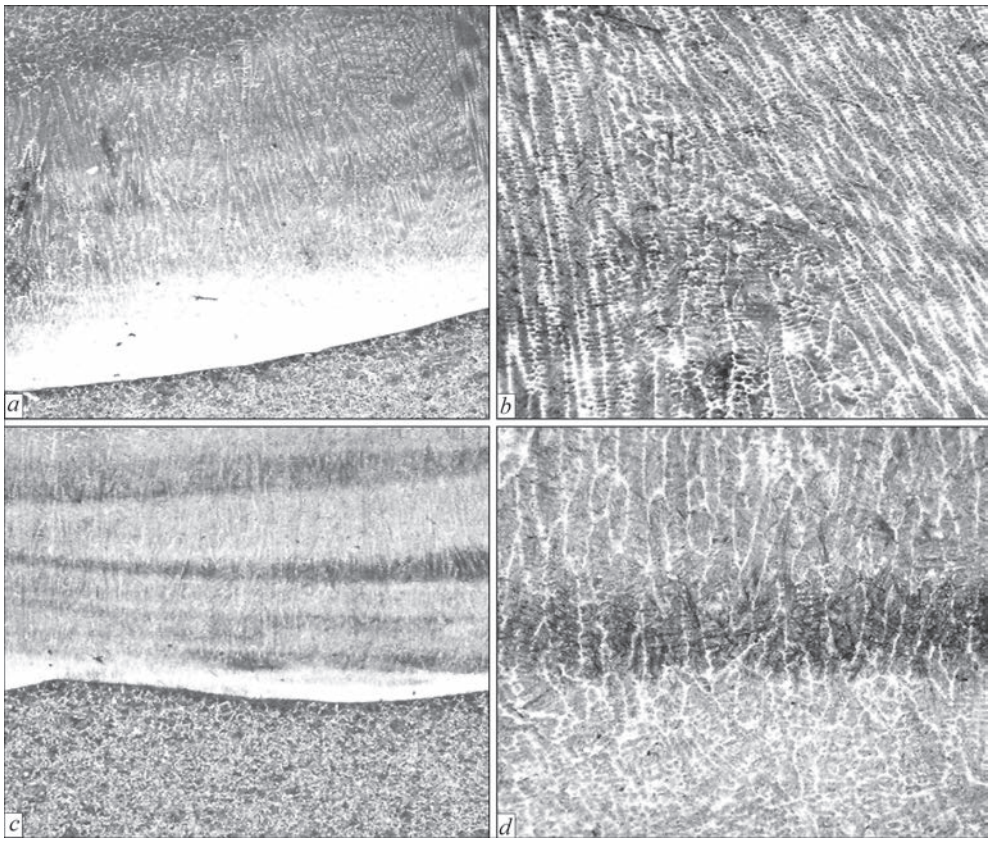

Figure 8. Microstructure of deposited metal of samples 7 (*a*, *b*) and 8 (*c*, *d*): *a*, *c* — fusion zone, ×20; *b*, *d* — deposited metal, ×100. Electrolytic etching in chromic acid. $U_{o.-c}$ = 20 V; *t* = 3–5 s (for sample numbers see Table 1)

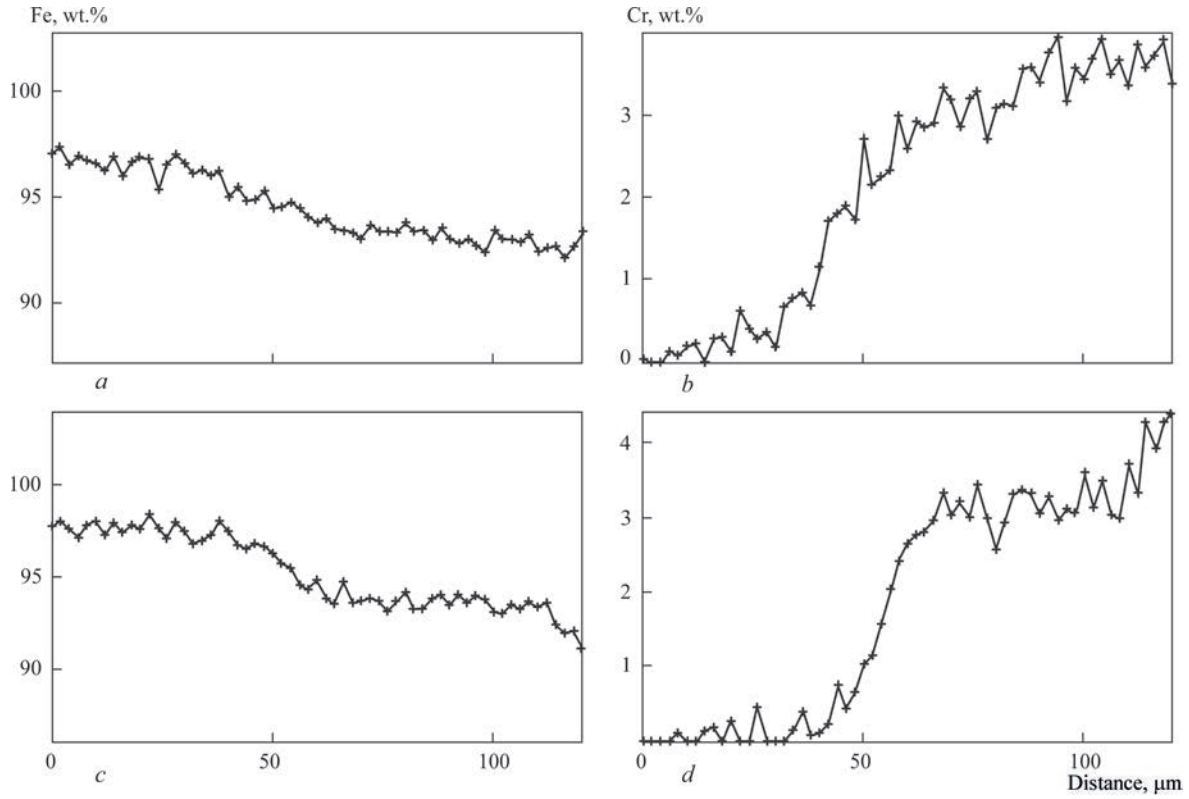

Figure 9. Fe (*a*, *c*) and Cr (*b*, *d*) distribution in the transition zone of sample 1 (*a*, *b*) and sample 2 (*c*, *d*)

Microstructure of deposited metal of sample 8 (V_d = 10 m/h; A = 40 mm; N = 32 min^{-1}) is dendritic-cellular (Figure 8, *c*, *d*). Cell diameter is 15–30 μm, crystallite width h_{cryst} is 30–40 μm, HAZ width is 600–800 μm. Chemical heterogeneity was detected over the entire surface of the deposited metal. There are precipitates along the boundaries of crystallites and cells. Microhardness in the light layer is *HV*1–6060–6130 MPa; in the heterogeneous region *HV*1–4840 MPa.

Methods of X-ray microanalysis, X-ray structure and metallographic analyses were used to study the chemical and structural heterogeneity of the deposited metal. Recording of linear distribution of alloying elements was performed at the distance of 600–700 μm from the deposited layer surface. Figure 9, *a–d* gives the curves of Fe and Cr distribution in the transition zone of samples 1 and 2 as an example.

Comparative analysis showed that the length of the transition zone becomes smaller at increase of oscillation frequency. So, at oscillation frequency of 28 min^{-1} the width of the transition zone is close to 35–40 μm, and at the frequency of 45 min^{-1} it is 20–25 μm (Table 2, samples 1 and 2). Similar results were obtained at analysis of the deposited bead microstructure in samples 1–8 (see above).

The fusion zone has a smooth concentration transition, and chemical microheterogeneity of the deposited metal is relatively small and is equal for chromium to Cr_{max}/Cr_{min} = 1.20–1.46; for molybdenum — to

Table 2. Influence of surfacing mode with wire oscillations on the microstructure and microheterogeneity of the deposited metal of samples 1–8 (see Table 1)

Sample number	Surfacing modes			Parameters of microstructure state			Cr and Mo chemical heterogeneity			
	V_d, m/h	A, mm	N, min^{-1}	D_{cell}, μm	Width of transition zone, μm	Microhardness *HV*1, MPa	Cr_{max}/Cr_{min}		Mo_{max}/Mo_{min}	
1	7	25	28	60–80/90–120	35–40	5420–6060	4.5/3.4	1.32	0.32/0.25	1.28
2*	7	25	45	30–40/70–90	20–25	5420–5480	4.8/3.9	1.23	0.40/0.33	1.21
3	7	40	18	50–60/70–80	30–35	6060–6130	3.4/2.3	1.47	0.42/0.32	1.31
4	7	40	32	40–50/60–80	15–20	5140–5400	3.1/2.2	1.41	0.35/0.28	1.25
5	10	25	28	25–35/25–50	35–40	6800	4.2/3.1	1.35	0.41/0.30	1.36
6	10	25	45	15–20/15–25	20–25	6700–6800	4.6/3.2	1.44	0.38/0.30	1.26
7	10	40	18	40–60/40–60	30–35	6400–6300	3.8/2.9	1.31	0.42/0.34	1.23
8	10	40	32	15–30/30–40	15–20	6340–6810	3.5/2.4	1.46	0.34/0.28	1.21

*Sample deposited in the optimum mode.

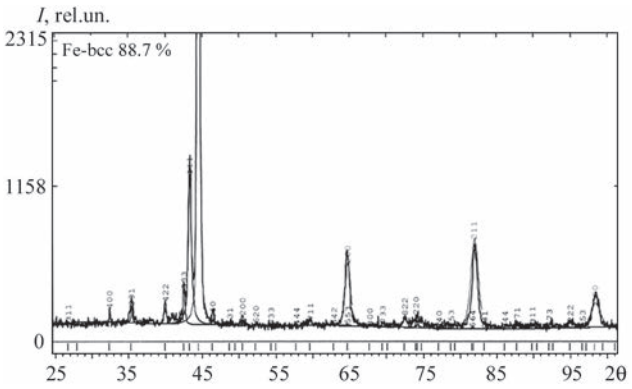

Figure 10. Phase composition of deposited metal of sample 2: Fe-bcc — 88.39 %; Fe-fcc — 8.11 %; Fe_3Mo_3C — 3.00 %; Cr_2C_3 — balance

Mo_{max}/Mo_{min} = 1.21–1.31. Increase of the frequency of electrode wire oscillations promotes producing a dispersed structure, more uniform distribution of alloying elements, «smoother» line of fusion of the deposited and base metal, as well as better mixing of the layers in the deposited metal. Hardness of the matrix base is 5140–6060 MPa. Carbides of Cr_7C_3, Fe_3C type and intermetallics of $Mo_5Cr_6Fe_{18}$ type were found in the deposited samples (Figure 10).

Approximately the same pattern is observed at increase of deposition rate to 10 m/h (Table 2, samples 5–8). In this case, increase of oscillation frequency reduces the width of the transition zone, chemical heterogeneity of the deposited metal is Cr_{max}/Cr_{min} = = 1.31–1.46 for chromium; and Mo_{max}/Mo_{min} = 1.21–1.36 for molybdenum. Hardness of the matrix base in this case is somewhat higher and equal to 6340–6810 MPa.

Conclusions

1. Increase of the frequency of electrode wire oscillations at the same amplitude and deposition rate leads to:

- improvement of deposited metal formation;
- improvement of mixing of the layers in the deposited metal; formation of a more dispersed structure;
- narrowing of the transition zone;
- more uniform distribution of alloying elements;
- more uniform nature of penetration and «smoothing» of the line of fusion of the deposited and base metal.

Here, it should be noted that these regularities practically do not change at increase of oscillation amplitude.

2. It was established that the best formation of the deposited metal, the smoothest and most uniform penetration are observed at electrode wire oscillation frequency N = 45 min^{-1}, electrode wire oscillation amplitude A = 25 mm and deposition rate V_d = 7 m/h.

The work was performed under the integrated program of the NAS of Ukraine «Problems of residual life and safe service of structures, constructions and machines» in 2016–2020.

1. Danilchenko, B.V., Shimanovsky, V.P., Voronchuk, A.P., Terpilo, V.N. (1989) Hard-facing of rapidly wearing parts by self-shielded flux-cored strips. *Avtomatich. Svarka*, **5**, 38–41 [in Russian].
2. Zhudra, A.P., Voronchuk, A.P., Fomakin, A.A., Veliky, S.I. (2009) New equipment for hard-facing of charging device bells and cups. *The Paton Welding J.*, **9**, 44–46.
3. Zhudra, A.P., Krivchikov, S.Yu., Petrov, V.V. (2010) Technology for wide-layer hard-facing of crankshafts. *Ibid.*, **2**, 32–35.
4. Gulakov, S.V., Burlaka, V.V. (2010) Mechanism of electrode oscillation for formation of deposited beads of complex shape. Vestnik Priazov. GTU. *Tekhnicheskie Nauki*, **20**, 181–186 [in Russian].
5. Spiridonov, N.V., Kudina, A.V., Kurash, V.V. (2013) Electric arc shielded-gas hard-facing of metal surfaces with oscillating electrode. *Nauka i Tekhnika*, **4**, 3–8 [in Russian].
6. Goloborodko, Zh.G., Dragan, S.V., Simutenkov, I.V. (2013) Automatic submerged-arc surfacing of structural steels with transverse high-frequency movements of electrode. *The Paton Welding J.*, **6**, 34–37.
7. Babinets, A.A., Ryabtsev, I.A., Kondratiev, I.A. et al. (2014) Investigation of thermal resistance of deposited metal designed for restoration of mill rolls. *Ibid.*, **5**, 16–20.
8. Ryabtsev, I.A., Babinets, A.A. (2015) Fatigue life of multilayer deposited specimens. *Svarochn. Proizvodstvo*, **4**, 15–19 [in Russian].

Received 09.09.2020